Dalton Transactions

Ligand Design of Zero-Field Splitting in Trigonal Prismatic Ni(II) Cage Complexes

Journal:	*Dalton Transactions*
Manuscript ID	DT-ART-06-2021-002156.R2
Article Type:	Paper
Date Submitted by the Author:	26-Jan-2022
Complete List of Authors:	Campanella, Anthony; Colorado State University, Chemistry Ozvat, Tyler; Colorado State University, Chemistry Zadrozny, Joseph; Colorado State University, Chemistry

RESEARCH ARTICLE

Ligand Design of Zero-Field Splitting in Trigonal Prismatic Ni(II) Cage Complexes

Received 00th January 20xx,
Accepted 00th January 20xx

DOI: 10.1039/x0xx00000x

Anthony J. Campanella[a], Tyler M. Ozvat[a], and Joseph M. Zadrozny*[a]

Complexes of encapsulated metal ions are promising potential metal-based electron paramagnetic resonance imaging (EPRI) agents due to zero-field splitting. Herein, we synthesize and magnetically characterize a series of five new Ni(II) complexes based on a clathrochelate ligand to provide a new design strategy for zero-field splitting in the encaged environment. UV-Vis and x-ray single-crystal diffraction experiments demonstrate slight physical and electronic structure changes as a function of the differing substituents. The consequence of these changes at the remote apical and sidearm positions of the encaging ligands is a zero-field splitting parameter (D) that varies over a large range of 11 cm^{-1}. These results demonstrate a remarkable flexibility of the zero-field splitting and electronic structure in nickelous cages and give a clear toolkit for modifying zero-field splitting in highly stable ligand shells.

Introduction

Electron paramagnetic resonance imaging (EPRI), the electron-spin analogue to conventional ^{1}H magnetic resonance imaging (MRI), is a potentially breakthrough technology[1–3] that can allow for non-invasive detection of various chemical markers (e.g. pH,[4–6] redox stress,[7–10] oxygenation[111–13]) indicative of biological distress and disease. Practical implementation of this technique requires low-frequency (< 1 GHz) microwaves to mitigate heating of water-rich biological tissue.[1,14] Thus, organic-radical based probes (the most common type)[1,11,15] require low magnetic fields for low-frequency analysis (**Fig. 1 Top Left**). Integration of EPRI with MRI would enable mapping chemical and anatomical information, a transformative diagnostic capability. Yet, common MRI scanners operate at 1.5 T and above, where high frequency microwaves (ca. 35 GHz) are necessary for function of organic radical probe systems (**Fig. 1 Top Left**). Thus, new types of probes are needed if EPRI is to merge with high-field MRI.

Metal ions in encaging ligands are a promising yet unexplored alternative imaging probe platform, which could provide access to novel reactivities (relative to radicals),[16–20] high chemical stabilities,[21] and ultimately new, tunable magnetic properties. Centerpiece among such magnetic properties is the feature of zero-field splitting (ZFS, characterized by the zero-field splitting parameter D) for high electron spin systems ($S > {}^1/_2$), which can uniquely produce low-frequency EPR resonances at high magnetic fields. Zero-field splitting, which is ubiquitous in $S > {}^1/_2$ metal ions, can therefore potentially surmount a key challenge imposed by using organic radicals for high-field EPRI (**Fig. 1 Top Right**).[22–24] Furthermore, this property could be leveraged for chemical sensing: changes in ligand field (e.g. from ligand-based protonation reactions or changes in metal-ion redox state) can result in modification of ZFS and thus induce changes in EPR signal intensity or frequency.

If we are to realize a new generation of metal-complex-based EPRI probes, it is therefore imperative to understand how to control ZFS in ligands that impose high chemical stability for metal complexes. One class of such molecules are clathrochelates, which consist of a metal ion encaged with a macrocyclic ligand that imposes high molecular stability.[21] We

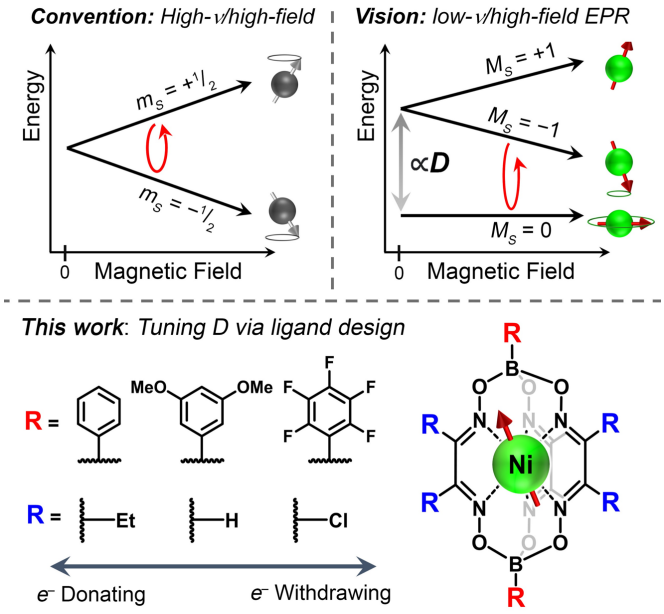

Fig. 1. (**Top**) Depiction of low-frequency EPR transitions in an organic radical ($S = {}^1/_2$) system, compared to that in a metal complex ($S = 1$) system. (**Bottom**) Overview of new work presented in this study.

[a] *Department of Chemistry, Colorado State University, Fort Collins, CO 80523, USA. Email: joe.zadrozny@colostate.edu*

Electronic Supplementary Information (ESI) available: Additional sample preparation details, characterization data, and spectroscopic details. See DOI: 10.1039/x0xx00000x

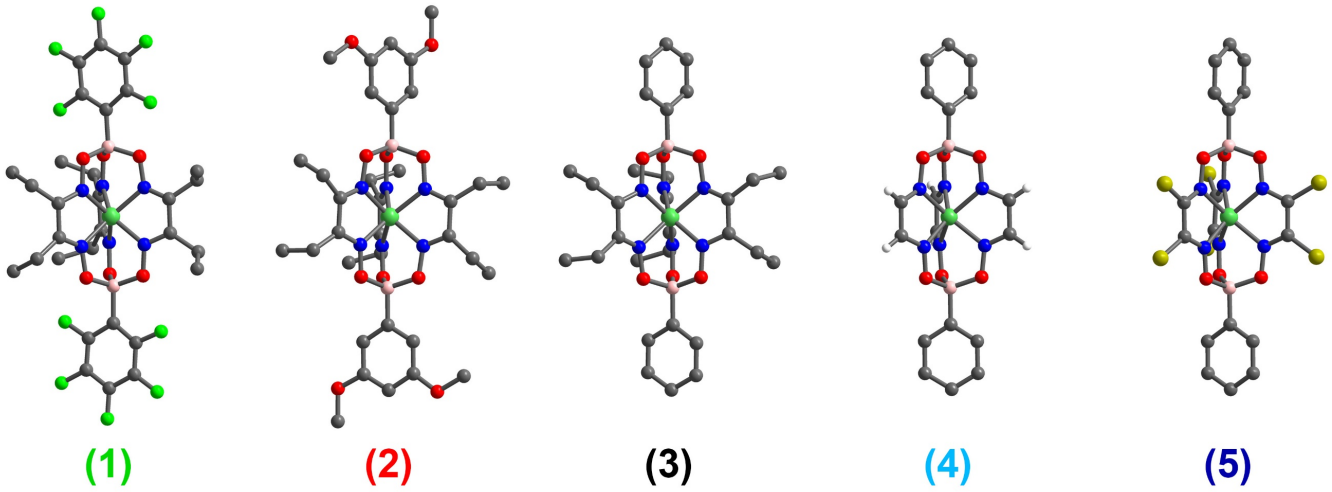

Fig. 2. Molecular structures of **1**-**5** as determined from single crystal X-ray diffraction. Light green, gray, blue, red, pink, neon green, dark yellow, and white spheres correspond to Ni, C, N, O, B, F, Cl, and H atoms, respectively. Most hydrogen atoms (except the sidearms of **4**) and a solvent molecule (in **3**) were omitted for clarity.

note that there is an abundance of strategies for controlling aspects of the electronic structure and magnetic properties of coordination complexes.[25,26] However, clathrochelate ligand frameworks only typically permit functional group changes multiple chemical units away from the central metal, where impacts on *D* may be suppressed. Thus, it is important to understand the basic design principles for controlling ZFS in clathrochelates and how to maximize the tunability of this parameter.

Towards that understanding, herein we report a synthetic, spectroscopic, magnetic, and computational study of a series of five new Ni(II) complexes that test how specific clathrochelate ligand functional groups influence ZFS. We hypothesized that modifying the locations of the functional groups and electron donating/withdrawing capabilities of the ligand would modulate ZFS, with the remaining question being the whether the magnitude of change would be large or small. To test this hypothesis, we prepared and analyzed five novel complexes, NiL1 (**1**), NiL2 (**2**), NiL3 (**3**), NiL4 (**4**), and NiL5 (**5**) (**Fig. 2**).§ The clathrochelate ligands (L1, L2, L3, L4, and L5) in this series vary the apical aryl rings and equatorial sidearms to test how the different groups affect the ZFS. We find that slight changes in the electronics and structure of the metal complexes from these functional groups enable a high tunability of *D*, 11 cm^{-1} over **1**-**5**. These results demonstrate a high possible degree of tunability for *D* in clathrochelate complexes via synthetic design.

Results and Discussion

The encapsulating boron-capped tris-dioximate ligands in **1**-**5** were synthesized via a template reaction with a Ni(II) source. This ligand design was first realized for Co(II,III)[27,28] and later expanded to Fe(II),[29] Ru(II),[30] and Mn(II).[31] To the best of our knowledge, this is the first synthetic report of Ni(II) in this basic ligand structure, and only one other Ni(II) structure of a ligand of this type found in the CSD.[32] Complexes **1**-**3** were synthesized by combining $NiCl_2$•$6H_2O$ and 3,4-hexanedionedioxime in dry MeCN, resulting in a maroon solution, followed by the addition of the respective aryl boronic acid and refluxing for 2-4 days to give the product as a light green powder. Complexes **4** and **5** were synthesized similarly with $NiCl_2$•DME (DME = dimethoxyethane), glyoxime (for **4**) or dichloroglyoxime (for **5**), and phenylboronic acid. Dry $MeNO_2$ was used as a solvent in these latter two syntheses due to the higher boiling point, which offsets the reported lesser reactivity of glyoxime and dichloroglyoxime.[33] Full synthetic details are described in the ESI (S3-S5).

The selected functional groups vary electron-donating and -withdrawing capabilities. Complexes **1**-**3** vary only the electron-withdrawing nature of the apical phenyl-borate unit and retain the same ethyl-sidearms. Complex **1** features perfluorinated phenyl rings and is the most electron-withdrawing system, followed by complex **2**, which bears axial phenyl groups with two methoxy groups in the 3- and 5-positions. Finally, **3** has no additional functional groups on the phenyl ring, suggesting that it is the least electron-withdrawing of the three. In complexes **3**-**5**, we instead vary the sidearms while keeping the apical phenyl group constant. Complex **3**, with ethyl groups, represents the most relative electron donating functional group in this series. In contrast, complex **4**, with hydrogen atoms and complex **5**, with chlorine atoms as sidearms, represent more electron-withdrawing systems. These qualitative assessments of the electron donating/withdrawing capabilities of the functional groups were made by comparing the appropriate Hammett constants for each substituent.[34]

All crystal structures indicate a nearly trigonal prismatic D_{3h} local symmetry for the NiN_6 coordination shell (**Figs. 2, 3a-b,** and **Tables S1-S5**). Average Ni–N distances are in a tight range, increasing from 1.996(9) Å (**1**) to 2.019(12) Å (**5**) across the series. These are longer than those found in the analogous Fe(II)[35,36] (near 1.910 Å) and Co(II)[28] (near 1.970 Å) complexes. The N–Ni–N bite angles range from 76.0(7)° to 78.4(4)°. All compounds are close to ideal trigonal prisms with average distortion angles (α, **Fig. 3b**) of 9.87(6)° (**1**), 5.83(8)° (**2**), 11.85(7)° (**3**), 11.63(8)° (**4**), and 6.60(2)° (**5**), where an ideal

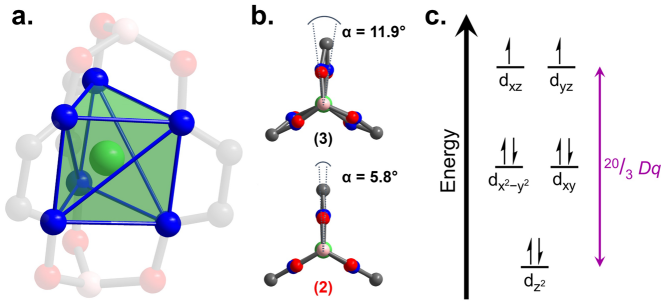

Fig. 3. (**a**) Molecular structure of **2** highlighting the uncommon nearly trigonal prismatic inner coordination geometry. Ethyl and phenyl groups were omitted for clarity. (**b**) Molecular structures of **2** and **3** viewed down the B–Ni–B axis showing the two extremes of the twist angle for **1**-**5** (denoted as α). Ethyl and phenyl groups were omitted for clarity. (**c**) 3*d*-orbital splitting diagram for a d^8 ion in an ideal trigonal prismatic geometry. $^{20}/_3Dq$ represents the energy gap between the top and bottom sets of orbitals.

trigonal prism would have α = 0° and an octahedron would have α = 60°. Continuous-Shape-Measurement analysis using the SHAPE 2.0 software[37,38] quantitively assessed any geometric distortions from SHAPE score of 0 corresponds to perfect alignment with the tested geometry. For the trigonal prismatic D_{3h} geometry, SHAPE scores for complexes **1**-**5** range from 0.26 to 0.78, while scores for octahedral geometries are much higher, between 11.55 and 15.58. These results indicate that all five complexes presented closely resemble perfect trigonal prisms, a relatively uncommon geometry for first-row metals in six-coordinate environments.[39] As one final point, the closest intermolecular Ni···Ni distances range from 5.797(2) Å in **4** to 9.571(2) Å in **1**.

Electronic absorption spectra were collected to identify changes in the Ni(II) ligand field as a function of ligand tuning. A broad, low-intensity peak was observed near 13,000 cm^{-1} for **1**-**4** and near 12,000 cm^{-1} for **5**. A higher intensity shoulder peak was also observed between 22,000 cm^{-1} (**5**) and 22,300 cm^{-1} (**2**), (**Fig. 4**). Peaks at energies above this latter set have been assigned as charge transfer bands in similar, isoelectronic Co(I) complexes.[33] Prior reports[40–42] of similar Ni(II) complexes in this geometry have made tentative assignments of the observed transitions, which enable comparisons between *Dq* values (where $^{20}/_3Dq$ for a trigonal prismatic complex is analogous to Δ_o, or 10*Dq,* for O_h geometries, (**Fig. 3c**) and ligand functional groups.[41]

For **1**-**5**, spectral deconvolution revealed two, low-energy peak in the absorbance spectra (**Figs. S1-S6**). The peaks occurred at 11,400 and 13,100 cm^{-1} for **1**, 11,400 and 13,100 cm^{-1} for **2**, 11,600 and 13,200 cm^{-1} for **3**, 11,700 and 13,400 cm^{-1} for **4**, and 9900 and 12,400 cm^{-1} for **5**. Using a Tanabe-Sugano diagram for a d^8 trigonal prismatic system,[41] we assigned the lowest energy peak to the spin-forbidden $^3A_2' \rightarrow {}^1E'$ transition, owing to its significantly lower intensity compared to the higher energy peak, which was subsequently assigned to the spin-allowed $^3A_2' \rightarrow {}^3E'(P)$ transition. The computed $^{20}/_3Dq$ and *B*

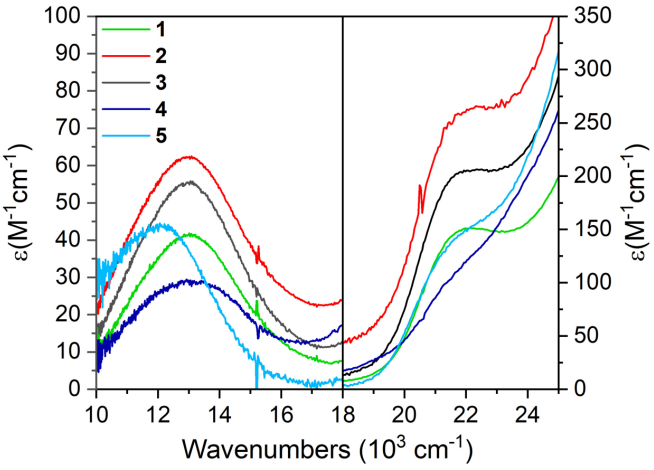

Fig. 4. Electronic absorption spectra of complexes **1**-**5** collected in CH_2Cl_2 with focus on the regions with the *d*-*d* transitions. Energies of peak absorption are discussed in the main text. High energy charge transfer bands were omitted for clarity. The sharp features near 15,200 cm^{-1} and near 20,500 cm^{-1} are artifacts of the instrument.

values are listed in **Table 1** and agree with those expected for species like **1**-**5**.[42]

For complexes **1**-**3** $^{20}/_3Dq$ decreased from 8,470 cm^{-1} (**3**), to 8,330 cm^{-1} (**1** and **2**) with the addition of more electron withdrawing ligand groups to the apical phenyl ring, implying a small decrease in the ligand field strength (**Fig. 3c**). To quantify the degree to which this change correlates with the electron withdrawing properties of ligand in **1**-**3**, we compared these results with the ^{11}B-NMR chemical shifts from the free boronic acid ligands. Spectra obtained of phenylboronic acid, 3,5-dimethoxyphenylboronic acid, and pentafluorophenylboronic acid produced ^{11}B chemical shifts at 29.18, 29.05, and 18.98 ppm, respectively (**Figs. S6-S9**). Though the trend is weak, we do see that an increase in the ^{11}B chemical shift of the free boronic acid is coupled with an increase in $^{20}/_3Dq$ between complexes **1**-**3**. These results illustrate how changing apical ligand electronics, which are relatively far away from the Ni ion, are still important in the ligand field for these encaging ligands.

In comparing **3**-**5**, where the sidearms were varied, we saw a more substantial change in $^{20}/_3Dq$, where it ranged from 7,250 cm^{-1} (**5**) to 8,530 cm^{-1} (**4**) and compound **3** fell in between at

Table 1. UV-Vis spectroscopic and spin Hamiltonian parameters determined for **1**-**5** through experimental (top) and computational (bottom) methods.

	1	**2**	**3**	**4**	**5**
$^{20}/_3Dq^a$	8,330	8,330	8,470	8,530	7,250
B^a	779	776	788	799	740
g_{iso}	1.997(3)	2.166(1)	2.033(1)	2.111(1)	2.157(4)
D^a	19.1(1)	19.8(2)	25.2(1)	29.4(4)	29.9(2)
$\|E\|^a$	1.3(1)	~0[b]	1.3(7)	6.2(1)	3.9(6)
$^{20}/_3Dq^a$	14,170	13,912	13,717	13,400	13,204
g_{iso}	2.176	2.183	2.176	2.177	2.192
D^a	33.6	47.7	27.2	30.7	39.5

[a]In units of cm^{-1}. [b]Refined value is 2.5×10^{-6}.

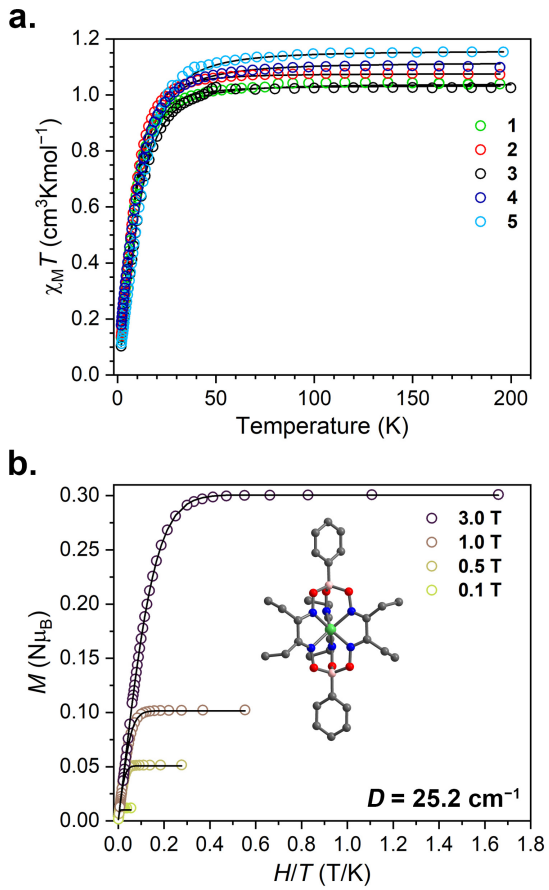

Fig. 5. (**a**) Variable temperature dc susceptibility data under 1.0 T applied dc magnetic field for powder samples of **1**-**5**. Solid lines are simulated data using the parameters generated from fitting the reduced magnetization data. (**b**) Reduced magnetization data and molecular structure of complex **3**. Solid lines are fits for the data generated using PHI. The spin Hamiltonian parameters (**Table 1**) are discussed in the main text. See the ESI for the reduced magnetization plots of **1**-**2**, **4**-**5** (**Figs. S6-S9**).

8,470 cm^{-1}. These results imply that there is a substantial decrease in the 3*d*-orbital splitting energy by adding Cl groups to the sidearms when compared to adding ethyl- or hydro-groups. However, these findings do not follow a clear trend with the electron donating/withdrawing character of the sidearm functional groups generally based on Hammett constants.[34] We note that although Hammett parameters are typically applied towards aromatic systems, in this instance, they only serve as a qualitative handle to make comparisons between the electronic effects of the ligand groups. We speculate the departure of the expected trend in **5** could be due to π-donation from the Cl groups into the conjugated binding units, an effect absent in the side-arms in **3** and **4**. In this picture, the π-donation may offset the changing σ-interactions accounted for when solely looking at the degree of electron withdrawing and donating ability.

Variable-temperature dc susceptibility data at 0.1, 0.5 1.0, and 3.0 T for **1**-**5** were analyzed to correlate changes in electronic structure to changes in zero-field splitting. Data collected at 1.0 T displayed as $\chi_M T$ vs. T revealed $\chi_M T$ values of 1.04, 1.07, 1.03, 1.11, and 1.15 cm^{3}K/mol at 300 K for **1**-**5**, respectively, (**Fig. 5a**) close to the expected value for an S = 1 system (1.00 cm^{3}K/mol, g = 2.00). With decreasing temperature, $\chi_M T$ remains relatively constant until about 50 K, where it begins to decrease substantially. The decrease in $\chi_M T$ with temperature is likely from zero-field splitting in the measured complexes. The multi-field reduced magnetization data were fit with PHI[43] to the following spin Hamiltonian:

$$\hat{H} = g\mu_B \boldsymbol{B}\hat{\boldsymbol{S}} + D\left(\hat{S}_z^2 - \frac{1}{3}S(S+1)\right) + E(\hat{S}_x^2 - \hat{S}_y^2).$$

Here, g is an isotropic g-factor ($g_x = g_y = g_z$), μ_B is the Bohr magneton, $\boldsymbol{B}$ is the applied magnetic field, $\hat{\boldsymbol{S}}$ is the electronic spin operator, D is the axial zero-field splitting parameter, and E is the rhombic zero-field splitting parameter. The values obtained from the fits are summarized in **Table 1**. As an additional measure of ZFS, we collected variable-field dc magnetometry on complexes **1**-**5** at 0.1 T, 0.5 T, and 3.0 T in temperatures ranging from 1.8 to 300 K. Reduced magnetization data from these measurements were fit in PHI to obtain spin Hamiltonian parameters g and D. The fits were relatively insensitive to E in both magnitude and sign. The values D were initially found to be 19.1(1) cm^{-1} (**1**), 19.8(2) cm^{-1} (**2**), 25.2(1) cm^{-1} (**3**), −29.4(4) cm^{-1} (**4**), and 29.9(2) cm^{-1} (**5**) and g values range from 1.997(3) to 2.166(1). The g values are within reported ranges of hexacoordinate Ni(II), however the D values are generally higher in magnitude than the typical –22 to +9.5 cm^{-1} range of O_h Ni(II) complexes.[44–48] To the best of our knowledge, this study represents the first experimental estimate of the tunability of D via ligand field modification in the D_{3h}, clathrochelate structure for Ni(II).

It stands out that **4** produced a fit with a negative sign for D. We note that fits of magnetic susceptibility data can give inaccuracies in D and E, particularly the signs of these parameters, where positive and negative D and E values can yield near-equal-quality data simulations.[49] Furthermore, as noted above, the susceptibility fits seemed insensitive to sign and magnitude of E. It is for these reasons that we report $|E|$ in **Table 1** rather than the sign.

Previous computational analyses of trigonal prismatic Ni(II) complexes,[50] as well as first-principle predictions based on the specific 3*d*-orbital excitations indicate that the sign of D should be positive.[51,52] This conclusion is also supported by $\chi_M T$ trending towards zero as the systems reach an M_s = 0 ground state. However, due to the possible inaccuracies in susceptibility determination of D, we pursued parallel-mode X-band EPR analyses of **1**-**5** to search for the $\Delta M_S = \pm 1$ intradoublet transition to provide additional experimental evidence to assign the sign of D. Analyses were conducted on **1**-**5** as 5 mM frozen glass solutions in a 1:1 (v/v) mixture chloroform and toluene at temperatures ranging from 4.5 K to 10 K. In the magnetic field of 0-600 mT, we failed to observe any signal that could be assigned to the complexes. At these lowest temperatures, observation of the intradoublet transition, with an intensity that increased with decreasing temperature, would have conclusively pinned the sign of D to be negative. Instead, there is no signal, even for **2**, which has a negligible E parameter. Owing to these spectroscopic and computational data, we confidently assign the zero-field splitting values as positive in **1**-**5** as noted in **Table 1**.

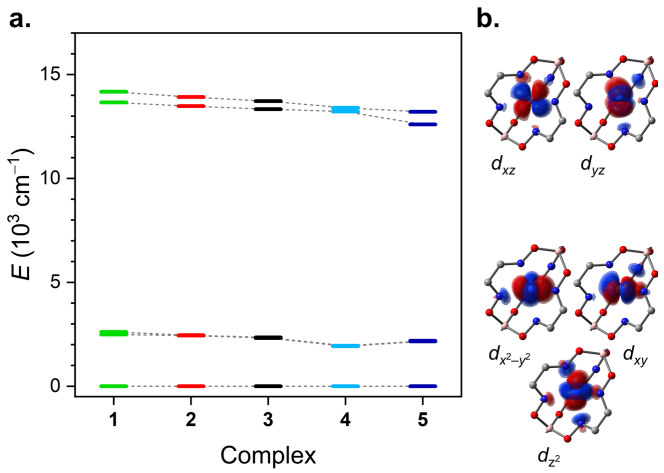

Fig. 6. (**a**) Energies of the 3*d* orbitals in **1**-**5** determined via AILFT. (**b**) Surface plots of the 3*d* orbitals corresponding to their relative energy levels in the energy level diagram.

Ab initio calculations based on single crystal structures allowed theoretical assessment of the electronic structures of **1**-**5** for comparison to experimental results (see ESI). Predictions of molecular orbital energies via ab initio ligand field theory (AILFT)[53,54] were extracted from Complete Active Space Self Consistent Field (CASSCF)[55,56] and n-electron valence state perturbation theory (NEVPT2)[57–59] calculations. The complete active space chosen for these computations included eight electrons and the five *d* orbitals of the Ni(II) ions, denoted as CAS(8,5). Calculations included 10 triplet and 15 singlet states, of which the $^3A_{2g}$ triplet ground state was lowest in energy. AILFT analyses reveal values of $^{20}/_3Dq$ for **1**-**5** at 14170, 13912, 13717, 13400, 13204 cm^{-1}, respectively. The results trend in a decreasing order from **1** to **5** (**Fig. 6**). For the series of apical-substituted groups (**1**-**3**), *reducing* the electron-withdrawing nature of the phenyl ring is coincident with lower $^{20}/_3Dq$. Conversely, for the series of sidearm-substituted groups (**3**-**5**), *enhancing* the electron-withdrawing nature of the dioximates follows with lower $^{20}/_3Dq$. We note the overestimation of the calculated $^{20}/_3Dq$ relative to the experimental values stems from the limited active space, however, the observed decrease in $^{20}/_3Dq$ is consistent with a progressively weaker σ-donating ligand resulting from the increased electron withdrawing ligand character on the side-arms, contributing to a weaker ligand field.[60] AILFT showed a steady decrease in $^{20}/_3Dq$ over the full series from **1**-**5** and specifically supports the experimental trend of decreasing $^{20}/_3Dq$ for **3**-**5**, driven by the electron-withdrawing capability of the ligand sidearm functional groups.

The foregoing electronic structures were also used to compute *D* for **1**-**5**. Results from CASSCF and NEVPT2 treatment gave all positive *D* values for **1**-**5** with magnitudes of 33.6, 47.7, 27.2, 30.7, and 39.5 cm^{-1}, respectively. No specific trend in *D* was accounted for by the apical substituents in series **1**-**3**. However, a notable increase in *D* in **3**-**5** matches the increased electron-withdrawing capabilities through the ligand sidearm.

The observed range of *D* in **1**-**5** stems from a range of contributions from the excited states. Of the 10 triplet states considered by CAS(8,5), only the four lowest-energy triplet excitations (within 10,000 to 13,000 cm^{-1}) contribute significantly to *D* (**Table S6, Figs. S13, S14**) For all five complexes, the first triplet excited states contribute to *D* with negative contributions that range from –2 to –12 cm^{-1}. The following three triplet excited states contribute positively to *D*, the largest of which range from +19 to +24 cm^{-1}. Strict consideration of triplet excitations showed mostly positive *D* contributions. Inclusion of singlet states was found to provide non-negligible contributions, despite the higher energies of these excitations (24,000 to 26,000 cm^{-1}). Of the 15 singlet states considered, only three affected *D* significantly, these being the second and third excited states (each near –5 cm^{-1}) and the fourth excited singlet state (between +15 to +19 cm^{-1}).

We note that the excited states are multiconfigurational, thus underlining the magnetic complexity of the zero-field splitting in these species (**Tables S7-S11**). Indeed, excitations between *d* orbitals of different $|m_l|$ value contribute to positive zero-field splitting magnitudes, whereas excitations within the same $|m_l|$ value are expected to contribute to a negative *D* (**Fig. S15**).[61,62] The fact that some of the excitations deviate from this rule emphasizes their multiconfigurational nature and the not-at-all trivial origin of the magnetic anisotropy.

The experimental results do not follow the predicted $^{20}/_3Dq$ and *D* values which warrants further discussion. Restriction of the active space to just the 3*d* orbitals via CAS(8,5) likely fails to capture all of the complexities of the electronic structures in **1**-**5**. Indeed, with the delocalized, conjugated structures, it is possible that including orbitals with more ligand character would ultimately drive the experimental trend, as has been previously suggested for Ni(II) chelate complexes.[45] The present outcome, that a metal-only approach does not perfectly reproduce the series, thus underlines the potential tunability of electronic structures and ZFS in through clathrochelate modification.

An overarching analysis of the zero-field splitting trends in **1**-**5** and the spectroscopic/structural/computational data makes it challenging to assign the trend to a specific electronic or structural feature. For one, the trends in $^{20}/_3Dq$ seem to weakly suggest a stronger ligand field correlates to a higher ZFS in **1**-**3**, while the opposite is true in **3**-**5** (with **4** lying outside this trend), the latter being supported by our computations. In a more practical sense, that argument then suggests a more electron withdrawing group favors a larger *D* value when placed on the sidearm whereas an opposite effect is seen in the apical positions. The typical expectation for zero-field splitting is that it will be greatest with weakest ligand field splitting,[51] for which the trends from **1**-**3** seem to be in defiance of.

A complicating feature in the analysis of the *D* trend is that the changes to the coordination geometries with functional group are minor,[63] but may be significant for the zero-field splitting.[50] From **1** to **5**, an increase in *D* is observed with an increase in the average Ni–N distance across the series with **1** showing the shortest Ni–N distances (*ca*. 1.996 Å) and lowest *D* value, and **5** showing the highest Ni–N distances (*ca*. 2.019 Å) and highest *D* value, respectively. The Ni–N distances are likely reflective of the ligand-field consequences of the different functional groups, where electron withdrawing groups enforce

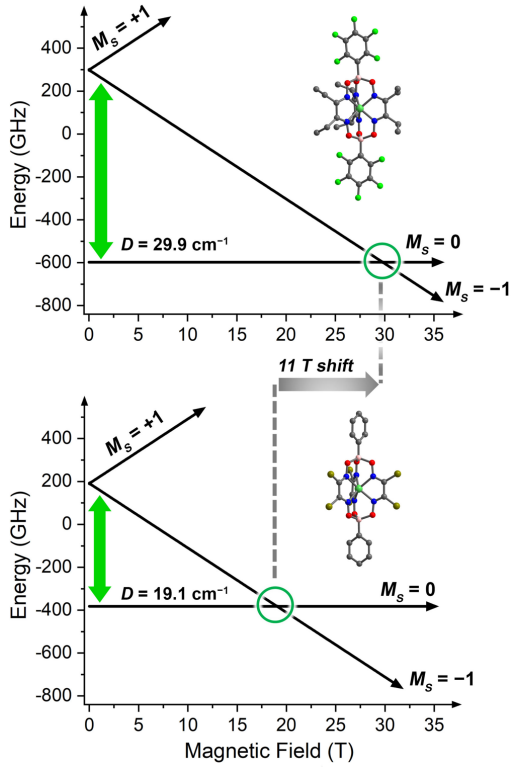

Fig.7. M_S-level energies for **1** and **5** (assuming magnetic field alignment with molecular z axis) showing the extent that *D* is tuned in this study. As a result of the change in *D*, the spin Hamiltonian parameters predict a *ca*. 11 T shift in the crossings of the M_S = 0 and M_S = –1 levels, demonstrating the tunability of fields for potential high-field/low-frequency EPR imaging studies.

weaker bonding, longer Ni–N distances, lower $^{20}/_{3}Dq$, and thus larger *D*. But, we also note that the apical functional groups could be inducing a change in the twist angle, α, of the trigonal prismatic ligand shell via steric forces around the congested B atom. Separate analyses suggest that α is the central parameter for affecting ZFS and electronic structure in similar complexes.[50,64] Yet there does not appear to be a correlation between α and *D* in our data. Owing to the foregoing points, it is thus challenging to attribute one sole feature to the modification of *D*, necessitating future studies to fully understand the variation.

Importantly, the variation in *D* that we observe here is dramatic for the relatively minor variations observed in the ligand shells of **1**-**5**. Large variations in *D* tend to result from substantial changes to the coordination shell. For example, large changes occur when donor atoms are directly swapped, as observed in the Co(II) complexes $[Co(EPh)_4]^{2-}$ (E = O, S, and Se), which vary 70 cm^{-1} in *D* as a function of E atom.[65] Second, large changes in geometry, e.g. changes in coordination number,[66] or conformation from square planar to tetrahedral,[67] can trigger high-amplitude modifications of *D*.[26] In the present system, we observe very slight change in bond distances (*ca.* 0.01 Å) and bond angles (*ca.* 5° for α), all within a nearly trigonal-prismatic, six-coordinate structure. Furthermore, these changes are imposed by varying function groups that are two and four bonds away from the Ni(II) ion, wherein any expected impact should be small. Yet, both experimental and computational evidence shows that these physical changes still exert a large effect on the zero-field splitting, even if the underlying electronic origin is still to be determined.

Finally, we used the spin-Hamiltonian parameters from **1** and **5** to calculate where safe, low-frequency transitions would potentially show up, because **1** and **5** are the two extremes of the series in terms of *D* (**Fig. 7**). For molecules with the magnetic field aligned perpendicular to the B···Ni···B axis of the molecule, 1 GHz transitions appear at 19.0 T (for **1**) and 29.8 T (for **5**). This is nearly an 11 T range and demonstrates a remarkable degree of tunability of the low-frequency transition as a function of ligand identity. However, note that the resonant fields of these low-frequency EPR transitions are considerably larger than the typical fields used in MRI (*ca*. 1.5 T) and preclinical (*ca.* 7 T) scanners.[68] In order to have the desired low-frequency transitions in those field ranges for an *S* = 1 system, *D* would have to be near 1.5 cm^{-1} for the former case, and 6.6 cm^{-1} for the latter case. Thus, there is a need to design the low-frequency EPR transition for lower fields in Ni(II) systems, as well as taking the learned design strategies and applying them towards other candidate EPRI molecular probes. Nevertheless, this striking degree of tunability suggests that will be possible with judicious ligand/metal selection.

Conclusions

In summary, we demonstrate a synthetic toolkit for finetuning the zero-field splitting in Ni(II) clathrochelate complexes. We found that judicious selection of axial and sidearm functional groups will modify ZFS over a relatively large, 11 cm^{-1} range. The significance of this range is underlined considering we do not directly modify the donor atom, but rather peripheral functional groups up to four bonds away from the metal. We note that there are several magnetostructural correlations for *D* and Ni(II),[42-46] but this study is, to the best of our knowledge, the first of its kind for the trigonal prismatic geometry.

The observations in this paper show that relatively tiny design changes to the encapsulating ligand shell can have dramatic impacts on ZFS, which has two important implications. First, the results highlight the possibility of engineering the operating field range for low-frequency EPR-based techniques by tuning *D*. A second implication of the sensitivity is that, if one engineered a pH-, redox- or other chemically responsive ligand field into a clathrochelate ligand, one could engender chemical sensitivity into any magnetic resonance spectroscopic property influenced by zero-field splitting. Toward applications of this type, including EPRI, we must first test whether the observed tunability carries over to the magnetic resonance properties of other metal ions and other spin states, e.g. *S* = $^{3}/_{2}$ Co(II) or *S* = $^{5}/_{2}$ Fe(III). Results from these efforts will be published in due course.

Conflicts of interest

There are no conflicts to declare.

Acknowledgements

We thank Prof. M. Reynolds and M. Roach for use of their mass spectrometer and experimental assistance. We also thank Prof. G. Miyake and C. Chrisman for their generous donation of ligand precursors. Lastly, we thank I. Moseley for assistance with magnetometry measurements. This research was performed with the support of Colorado State University (CSU) and the NIH (R21-EB027293) (A. J. C., T. M. O., J. M. Z.). Magnetometry, EPR, and standard molecular characterization were performed at the CSU Analytical Resources Core, which is supported by an NIH-SIG award (1S10OD021814-01) and the CSU-CORES Program. Computational resources are enabled by the Catalysis Collaboratory for Light-activated Earth Abundant Reagent (C-CLEAR), which is supported by the National Science Foundation and the Environmental Protection Agency through the Networks for Sustainable Molecular Design and Synthesis (Grant CHE-1339674) at CSU, Fort Collins.

Notes and references

§ L1 = (1,8-bis(pentafluorophenyl)-4,5,11,12,17,18-hexaethyl-2,7,9,14,15,20-hexaoxa-3,6,10,13,16,19-hexaaza-1,8-diboratabicyclo[6.6.6]icosa-3,5,10,12,16,18-hexaene); L2 = (1,8-bis(pentafluorophenyl)-4,5,11,12,17,18-hexaethyl-2,7,9,14,15,20-hexaoxa-3,6,10,13,16,19-hexaaza-1,8-diboratabicyclo[6.6.6]icosa-3,5,10,12,16,18-hexaene); L3 = (1,8-bisphenyl-4,5,11,12,17,18-hexaethyl-2,7,9,14,15,20-hexaoxa-3,6,10,13,16,19-hexaaza-1,8-diboratabicyclo[6.6.6]icosa-3,5,10,12,16,18-hexaene); L4 = (1,8-bisphenyl-2,7,9,14,15,20-hexaoxa-3,6,10,13,16,19-hexaaza-1,8-diboratabicyclo[6.6.6]icosa-3,5,10,12,16,18-hexaene); L5 = (1,8-bisphenyl-4,5,11,12,17,18-hexachloro-2,7,9,14,15,20-hexaoxa-3,6,10,13,16,19-hexaaza-1,8-diboratabicyclo[6.6.6]icosa-3,5,10,12,16,18-hexaene)

1 L. J. Berliner, Ed., *In Vivo EPR (ESR): Theory and Application*, Springer US, 2003.
2 J. P. Klare, *Biomed. Spectrosc. Imaging*, 2012, 101–124.
3 S. Colacicchi, M. Ferrari and A. Sotgiu, *Int. J. Biochem.*, 1992, **24**, 205–214.
4 M. A. Voinov, C. T. Scheid, I. A. Kirilyuk, D. G. Trofimov and A. I. Smirnov, *J. Phys. Chem. B*, 2017, **121**, 2443–2453.
5 M. A. Voinov, J. F. Polienko, T. Schanding, A. A. Bobko, V. V. Khramtsov, Y. V. Gatilov, T. V. Rybalova, A. I. Smirnov and I. A. Grigor'ev, *J. Org. Chem.*, 2005, **70**, 9702–9711.
6 D. I. Potapenko, M. A. Foster, D. J. Lurie, I. A. Kirilyuk, J. M. S. Hutchison, I. A. Grigor'ev, E. G. Bagryanskaya and V. V. Khramtsov, *J. Magn. Reson.*, 2006, **182**, 1–11.
7 G. L. Caia, O. V. Efimova, M. Velayutham, M. A. El-Mahdy, T. M. Abdelghany, E. Kesselring, S. Petryakov, Z. Sun, A. Samouilov and J. L. Zweier, *J. Magn. Reson.*, 2012, **216**, 21–27.
8 T. Mikuni, G. He, S. Petryakov, M. M. Fallouh, Y. Deng, R. Ishihara, P. Kuppusamy, M. Tatsuta and J. L. Zweier, *Cancer Res.*, 2004, **64**, 6495–6502.
9 F. Hyodo, R. Murugesan, K. Matsumoto, E. Hyodo, S. Subramanian, J. B. Mitchell and M. C. Krishna, *J. Magn. Reson.*, 2008, **190**, 105–112.
10 B. Epel, S. V. Sundramoorthy, M. Krzykowska-Serda, M. C. Maggio, M. Tseytlin, G. R. Eaton, S. S. Eaton, G. M. Rosen, J. P. Y. Kao and H. J. Halpern, *J. Magn. Reson.*, 2017, **276**, 31–36.
11 Gareth R. Eaton, Sandra S. Eaton, and Keiichi Ohno, Eds., *EPR Imaging and in Vivo EPR*, CRC Press, 1991.
12 F. Demsar, T. Walczak, P. D. Morse, G. Bačić, Z. Zolnai and H. M. Swartz, *J. Magn. Reson. 1969*, 1988, **76**, 224–231.
13 H. M. Swartz, A. B. Flood, P. E. Schaner, H. Halpern, B. B. Williams, B. W. Pogue, B. Gallez and P. Vaupel, *Physiol. Rep.*, 2020, **8**, e14541.
14 R. T. Hitchcock, *Radio-frequency and Microwave Radiation*, AIHA, 2004.
15 P. Danhier and B. Gallez, *Contrast Media Mol. Imaging*, 2015, **10**, 266–281.
16 Y. Z. Voloshin, O. A. Varzatskii, T. E. Kron, V. K. Belsky, V. E. Zavodnik, N. G. Strizhakova, V. A. Nadtochenko and V. A. Smirnov, *J. Chem. Soc. Dalton Trans.*, 2002, 1203–1211.
17 Y. Z. Voloshin, O. A. Varzatskii, T. E. Kron, V. K. Belsky, V. E. Zavodnik, N. G. Strizhakova and A. V. Palchik, *Inorg. Chem.*, 2000, **39**, 1907–1918.
18 Y. Z. Voloshin, A. Y. Lebedev, V. V. Novikov, A. V. Dolganov, A. V. Vologzhanina, E. G. Lebed, A. A. Pavlov, Z. A. Starikova, M. I. Buzin and Y. N. Bubnov, *Inorg. Chim. Acta*, 2013, **399**, 67–78.
19 O. M. Planes, R. Scopelliti, F. Fadaei-Tirani and K. Severin, *Z. Anorg. Allg. Chem.*, 2021, **647**, 1065–1069.
20 G. Cecot, M. T. Doll, O. M. Planes, A. Ramorini, R. Scopelliti, F. Fadaei-Tirani and K. Severin, *Eur. J. Inorg. Chem.*, 2019, **2019**, 2972–2976.
21 Y. Voloshin, I. Belaya and R. Krämer, in *Cage Metal Complexes*, Springer International Publishing, Cham, 2017, pp. 1–100.
22 J. S. Griffith, *The Theory of Transition-Metal Ions*, Cambridge University Press, 1964.
23 B. N. Figgis and M. A. Hitchman, *Ligand field theory and its applications*, Wiley-VCH, 2000.
24 A. J. Campanella, M.-T. Nguyen, J. Zhang, T. Ngendahimana, W. E. Antholine, G. R. Eaton, S. S. Eaton, V.-A. Glezakou and J. M. Zadrozny, *Dalton Trans.*, 2021, 5342–5350.
25 S. Gómez-Coca, D. Aravena, R. Morales and E. Ruiz, *Coord. Chem. Rev.*, 2015, **289–290**, 379–392.
26 J. M. Frost, K. L. M. Harriman and M. Murugesu, *Chem. Sci.*, 2016, **7**, 2470–2491.
27 D. R. Boston and N. J. Rose, *J. Am. Chem. Soc.*, 1968, **90**, 6859–6860.
28 E. C. Lingafelter, G. A. Zakrzewski and C. A. Ghilardi, *J. Am. Chem. Soc.*, 1971, **93**, 4411–4415.
29 S. C. Jackels and N. J. Rose, *Inorg. Chem.*, 1973, **12**, 1232–1237.
30 J. G. Muller, K. J. Takeuchi and J. J. Grzybowski, *Polyhedron*, 1989, **8**, 1391–1399.
31 W.-Y. Hsieh and S. Liu, *Inorg. Chem.*, 2006, **45**, 5034–5043.
32 Yongteng Wei, *CSD Commun.*, DOI: 10.5517/ccdc.csd.cc20mgjn.
33 Y. Z. Voloshin, O. A. Varzatskii, V. V. Novikov, N. G. Strizhakova, I. I. Vorontsov, A. V. Vologzhanina, K. A. Lyssenko, G. V. Romanenko, M. V. Fedin, V. I. Ovcharenko and Y. N. Bubnov, *Eur. J. Inorg. Chem.*, 2010, **34**, 5401–5415.
34 Corwin. Hansch, A. Leo and R. W. Taft, *Chem. Rev.*, 1991, **91**, 165–195.
35 Y. Z. Voloshin, N. A. Kostromina and A. Y. Nazarenko, *Inorg. Chim. Acta*, 1990, **170**, 181–190.
36 V. V. Novikov, I. V. Ananyev, A. A. Pavlov, M. V. Fedin, K. A. Lyssenko and Y. Z. Voloshin, *J. Phys. Chem. Lett.*, 2014, **5**, 496–500.

37 S. Alvarez, P. Alemany, D. Casanova, J. Cirera, M. Llunell and D. Avnir, *Coord. Chem. Rev.*, 2005, **249**, 1693–1708.
38 S. Alvarez, D. Avnir, M. Llunell and M. Pinsky, *New J. Chem.*, 2002, **26**, 996–1009.
39 E. Cremades, J. Echeverría and S. Alvarez, *Chem. – Eur. J.*, 2010, **16**, 10380–10396.
40 W. O. Gillum, R. A. D. Wentworth and R. F. Childers, *Inorg. Chem.*, 1970, **9**, 1825–1832.
41 R. A. D. Wentworth, *Coord. Chem. Rev.*, 1972, **9**, 171–187.
42 J. C. Knight, S. Alvarez, J. A. Angelo, P. G. Edwards and N. Singh, *Dalton Trans.*, 2010, **39**, 3870–3883.
43 N. F. Chilton, R. P. Anderson, L. D. Turner, A. Soncini and K. S. Murray, *J. Comput. Chem.*, 2013, **34**, 1164–1175.
44 P. J. Desrochers, C. A. Sutton, M. L. Abrams, S. Ye, F. Neese, J. Telser, A. Ozarowski and J. Krzystek, *Inorg. Chem.*, 2012, **51**, 2793–2805.
45 G. Charron, E. Malkin, G. Rogez, L. J. Batchelor, S. Mazerat, R. Guillot, N. Guihéry, A.-L. Barra, T. Mallah and H. Bolvin, *Chem. – Eur. J.*, 2016, **22**, 16850–16862.
46 S. Gómez-Coca, E. Cremades, N. Aliaga-Alcalde and E. Ruiz, *Inorg. Chem.*, 2014, **53**, 676–678.
47 D. Schweinfurth, J. Krzystek, I. Schapiro, S. Demeshko, J. Klein, J. Telser, A. Ozarowski, C.-Y. Su, F. Meyer, M. Atanasov, F. Neese and B. Sarkar, *Inorg. Chem.*, 2013, **52**, 6880–6892.
48 J. Titiš and R. Boča, *Inorg. Chem.*, 2010, **49**, 3971–3973.
49 R. Boča, *Coord. Chem. Rev.*, 2004, **248**, 757–815.
50 N. Suaud, G. Rogez, J.-N. Rebilly, M.-A. Bouammali, N. Guihéry, A.-L. Barra and T. Mallah, *Appl. Magn. Reson.*, 2020, **51**, 1215–1231.
51 D. Dai, H. Xiang and M.-H. Whangbo, *J. Comput. Chem.*, 2008, **29**, 2187–2209.
52 A. Sarkar, S. Dey and G. Rajaraman, *Chem. – Eur. J.*, 2020, **26**, 14036–14058.
53 S. K. Singh, J. Eng, M. Atanasov and F. Neese, *Coord. Chem. Rev.*, 2017, **344**, 2–25.
54 M. Atanasov, J. M. Zadrozny, J. R. Long and F. Neese, *Chem. Sci.*, 2012, **4**, 139–156.
55 F. Aquilante, T. B. Pedersen, R. Lindh, B. O. Roos, A. Sánchez de Merás and H. Koch, *J. Chem. Phys.*, 2008, **129**, 024113.
56 P.-Å. Malmqvist and B. O. Roos, *Chem. Phys. Lett.*, 1989, **155**, 189–194.
57 C. Angeli, R. Cimiraglia, S. Evangelisti, T. Leininger and J.-P. Malrieu, *J. Chem. Phys.*, 2001, **114**, 10252–10264.
58 C. Angeli, R. Cimiraglia and J.-P. Malrieu, *Chem. Phys. Lett.*, 2001, **350**, 297–305.
59 C. Angeli, R. Cimiraglia and J.-P. Malrieu, *J. Chem. Phys.*, 2002, **117**, 9138–9153.
60 F. Shao, B. Cahier, N. Guihéry, E. Rivière, R. Guillot, A.-L. Barra, Y. Lan, W. Wernsdorfer, V. E. Campbell and T. Mallah, *Chem. Commun.*, 2015, **51**, 16475–16478.
61 R. Ruamps, L. J. Batchelor, R. Maurice, N. Gogoi, P. Jiménez-Lozano, N. Guihéry, C. de Graaf, A.-L. Barra, J.-P. Sutter, and T. Mallah, *Chem. – Eur. J.,* 2013, **19**, 950–956.
62 R. Ruamps, L. J. Batchelor, R. Guillot, G. Zakhia, A.-L. Barra, W. Wernsdorfer, N. Guihéry, and T. Mallah, *Chem. Sci.* 2014, **5**, 3418-3424.
63 S. A. Kubow, K. J. Takeuchi, J. J. Grzybowski, A. J. Jircitano and V. L. Goedken, *Inorg. Chim. Acta*, 1996, **241**, 21–30.
64 R. Ruamps, R. Maurice, L. Batchelor, M. Boggio-Pasqua, R. Guillot, A. L. Barra, J. Liu, E.-E. Bendeif, S. Pillet, S. Hill, T. Mallah and N. Guihéry, *J. Am. Chem. Soc.*, 2013, **135**, 3017–3026.
65 J. M. Zadrozny, J. Telser and J. R. Long, *Polyhedron*, 2013, **64**, 209–217.
66 P.-H. Lin, N. C. Smythe, S. I. Gorelsky, S. Maguire, N. J. Henson, I. Korobkov, B. L. Scott, J. C. Gordon, R. T. Baker and M. Murugesu, *J. Am. Chem. Soc.*, 2011, **133**, 15806–15809.
67 D. Lomjanský, C. Rajnák, J. Titiš, J. Moncoľ, L. Smolko and R. Boča, *Inorg. Chim. Acta.*, 2018, **483**, 352–358.
68 P. V. Prasad, Ed., *Magnetic Resonance Imaging: Methods and Biologic Applications*, Humana Press, Totowa, NJ, 2006.

